Kinetics of Poly(ethylene oxide) Crystallization from Solution: Temperature and Molecular Weight Dependence

Ni Ding† and Eric J. Amis*

Department of Chemistry, University of Southern California, Los Angeles, California 90089-0482

Received October 24, 1989; Revised Manuscript Received February 4, 1991

ABSTRACT: The rate of crystal growth from dilute solutions of poly(ethylene oxide) (PEO) of high and intermediate molecular weight has been investigated by utilizing a new seeding technique in conjunction with dynamic light scattering. Crystallization of polymers in a dilute solution is initiated by the addition of seed crystals and the growth kinetics are monitored by repetitive measurements of diffusion coefficients of crystal particles. The crystal growth rate can be extracted from the linear plot of inverse decay constant of scattering particles vs time. It has been found that the temperature influence on crystal growth kinetics in terms of log G vs $1/T\Delta T$ depends on the choice of $T_d°$. Regardless of the exact values of $T_d°$ used for the range of molecular weight samples, it is found that for high PEO molecular weights ($>3 \times 10^5$) a transition could be recognized in the dependence of the growth rate on the extent of supercooling. No such transition is found for intermediate ($<3 \times 10^5$) molecular weight PEO. At constant supercooling, the growth rate generally increases with polymer molecular weight over the range from 5.63×10^4 to 7.7×10^5.

Introduction

Studies of the molecular weight and temperature dependence of polymer crystal growth from dilute solution can play an important role in elucidating the mechanisms by which polymers in general crystallize. The first theoretical description of crystallization kinetics was based on the work of Avrami as an adaptation of formulations intended for metallurgy to the needs of polymer crystallization.[1] The two Avrami parameters derived from the treatment are characteristic of crystallization mechanisms that lead to differing dimensionality in the crystallization of morphologically distinct crystals. The parameters, and the theory, provide little insight however as to the molecular organization of the crystalline regions or the crystal evolution.

The kinetic nucleation theory has emerged as a promising framework for describing and understanding isothermal crystallization rates for linear polymers in quiescent melts or dilute solution.[2-4] In the kinetic nucleation theory there are three regimes of crystal growth, which are controlled by competing nucleation and growth processes. The first regime (I) describes a single nucleation per substrate length, L, where the nucleation rate, i, is slower than the substrate completion rate, g. The crystal growth rate is given by $G_I = biL$, where b is the thickness of a crystalline stem. In the second regime (II), multiple nucleation occurs on the growth face as the nucleation rate is roughly equivalent to or greater than the substrate completion rate. The crystal growth rate follows the equation of $G_{II} = b(2ig)^{1/2}$. The final regime (III) is a state of rapid polynucleation growth where nucleation occurs so rapidly that the separation of niches on the substrate that characterizes regime II approaches the width of a single stem.

According to kinetic nucleation theory the crystal growth rate can be expressed as

$$G_i = \frac{C_i}{N^\alpha} \exp\left(\frac{-U^*}{R(T-T_\infty)}\right) \exp\left(\frac{-K_g(i)}{T\Delta Tf}\right) \qquad i = \text{I, II, III} \tag{1}$$

where C_i's are preexponential factors for the three regimes, N is the degree of polymerization, α is an exponent predicted[3] to be in the range 1.33-1.5 for regime I and 1.17-1.25 for regime II, U^* is the activation energy for "reeling in" the polymer chain, which is postulated[3,5] to occur by a mechanism of steady-state reptation, and ΔT is the difference between the equilibrium melting temperature, $T_m°$, and the crystallization temperature, T; T_∞ is usually within about 5-10 K of being 50 K below T_g. Neither T_g or U^* is a strong function of the molecular weight for moderate to high molecular weights. The temperature correction factor f is given by $f = 2T/(T_m° + T)$. It has little effect at low undercooling. $K_g(i)$ represents the nucleation constant for the three regimes. The constants are related as $K_g(\text{I}) = 2K_g(\text{II}) = K_g(\text{III})$ and

$$K_g(\text{I}) = 4b\sigma\sigma_e T_m°/k\,\Delta h_f \tag{2}$$

where σ and σ_e are the lateral and fold surface free energies, respectively, k is Boltzmann's constant, and Δh_f is the heat of fusion of the polymer crystal. For crystals grown from solution, eq 1 is modified to read

$$G_i \sim \frac{c^\gamma}{N^\alpha} \exp\left(\frac{-U^*}{RT}\right) \exp\left(\frac{-K_g(i)}{T\Delta T}\right) \qquad i = \text{I, II} \tag{3}$$

where c is the polymer concentration with a γ power dependence that depends on the regime, U^* is the diffusion activation energy of the dissolved polymer, and α is here predicted to be positive and near 0.5 under a snakelike, but nonreptative, model for the polymer chain.[6] For crystallization from dilute solution, the side-to-side motion of the chain, which is allowed by the presence of solvent molecules, eliminates the reptation tube from the melt model. In dilute solution U^* is much smaller than $K_g(\text{I})$ such that the first exponential term can be treated as a constant over the ΔT of 30 K which can typically be attained in solution studies. With fixed N and c, plots of log G vs $1/T\Delta T$ are directly analogous to the characteristically kinked regime transition plots that have been used by Hoffman and co-workers[2] to demonstrate the existence of nucleation regimes in crystallizations from polymer melts.

In melts, regime transitions have been shown for polyethylene,[2,7] poly(ethylene oxide),[8,9] poly(*p*-phenylene sulfide),[10] and other polymers.[11,12] Solution crystallization experiments are not as numerous and are difficult. Past

† Present address: Research Laboratories, Rohm and Haas, Spring House, PA 19477.

0024-9297/91/2224-3906$02.50/0

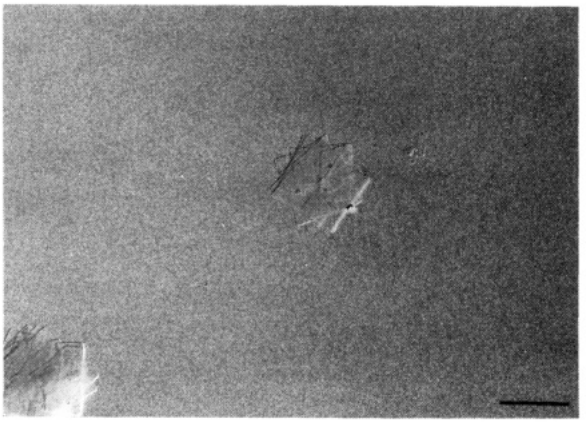

Figure 1. Transmission electron micrograph of PEO 105 crystals grown at T = 17 °C. Bar 1 μm.

solution work has used microscopy,[13-15] small-angle static light scattering,[16,17] and turbidity measurements.[18,19] The recent study on the system of polyethylene in hexadecane or tetradecanol[19] provided the first evidence of regime transitions similar to those observed in melt crystallization. Recently a new technique for crystal growth studies has been developed that provides real time in situ measurements of crystal size in solution by dynamic light scattering (DLS).[20,21] The method has been applied to the crystallization of poly(ethylene oxide) (PEO) from toluene solutions[20] and in combination with a new method for preparing seed crystals[21] has been shown to yield reproducible results over broad ranges of polymer molecular weight, concentration, and solution supercooling.

In this investigation we have used this new DLS technique to systematically study the temperature and molecular weight dependence of PEO crystallization kinetics from toluene solutions. The technique requires measurements be initiated on dilute solutions, which are prepared to be free of heterogeneous nucleation sites, mostly dirt particles or catalyst residuals, and uses a seeding technique that provides controlled initiation of crystal growth without temperature jumps or thermal shocks.

In our previous work, which included electron microscopy (Figure 1), it was found that crystals grown by this method developed as layered clusters of diamond forms.[21] Similar cluster morphology was reported by Organ and Keller in their work on polyethylene (PE) crystals grown at higher temperature or from particular solvents (e.g., hexyl acetate and dodecanol).[22] The clusters appeared to consist of several staggered layers. Since a very similar structure was observed for the seeds, it was suggested that the crystals are connected at their centers and concentrically grow in two dimensions. The crystallographic growth face is flat, and no obvious morphological change was observed as temperature was varied.

The experiments reported here provide some of the most detailed solution kinetics studies to date. These studies are not isolated however. Following the observation of the regime I to II transition for polyethylene solutions, it will not be surprising to also see it for PEO. Like PE, PEO does not have tacticity, and its backbone is even more flexible. Melt crystallization work on PEO provides valuable comparative data.[8,9] On the other hand, previous careful work with low molecular weight PEO has demonstrated integer folding[23-26] and evidenced an entropically controlled rough surface crystallization mechanism.[27] While these phenomena are very interesting, we have, for this work, chosen to avoid these complications by focusing on intermediate and high molecular weight PEO.

Table I
Molecular Characterization of PEO Fractions

sample	M_p[a]	M_w/M_n	N_w
PEO 56	5.63×10^4	1.05	1340
PEO 105	1.05×10^5	1.03	2460
PEO 160	1.60×10^5	1.05	3820
PEO 325	3.25×10^5	1.06	7830
PEO 770	7.70×10^5	1.12	19600

[a] GPC molecular weight.

Experimental Section

PEO standards with molecular weights from 5.63×10^4 to 7.70×10^5 and with very narrow molecular weight distributions were obtained from Polymer Laboratories (Amherst, MA). The characteristics of the five samples are given in Table I. All polymers were dried and stored over P_2O_5. Details of the preparation of the polymer solutions and the seed suspension have been described previously.[20,21] Reagent grade toluene was dried with Na and molecular sieves and was freshly distilled. Sample clarification was accomplished by filtration of the warm (~50 °C) solutions directly into scattering cells in a laminar flow hotbox. All solutions were 0.01% by weight of PEO. Seed crystals were prepared by rapidly cooling filtered and sealed solutions to liquid nitrogen temperatures. As observed previously,[21] warming these frozen samples to room temperature gave suspensions of small and stable seeds.

The dynamic light scattering technique was used to measure the crystal growth. A fixed scattering angle of 40° was used (after the correct q^2 angular dependence of the scattering had been verified at several points along the growth curve) for all measurements. The crystallization temperature was maintained by regulating the temperature of the refractive index matching bath to ±0.03 °C for the duration of each run. The temperature was measured with a thermistor thermometer (Cole Palmer Model 8502), which was calibrated to provide readings of temperature in the scattering cell. The goniometer (Brookhaven SM-200) and correlator (Brookhaven 2030AT) used for the DLS have been described previously.[20,28] Solutions and seed suspensions were preequilibrated at the desired supercooling temperature prior to mixing. Because the scattering solutions were dust-free, no spontaneous primary nucleation occurs for the temperature ranges covered in this investigation.

To initiate crystal growth an aliquot of seed suspension was added to the polymer solution. Depending on the crystallization temperature, 75 μL or less of seed suspension per gram of polymer solution was used. DLS correlation functions were repeatedly accumulated, each for a duration sufficient to obtain reasonable statistics (usually 1–2 min). The crystal growth was usually monitored until the crystals reached a stable final size (constant correlation function decay time). This occurs when the polymer in solution is exhausted. For large supercooling such that growth rates were very rapid, fewer seeds were used in order to prolong the period of crystal growth and measurement. Measured growth rates were independent of the amount of seeds used to initiate crystallization.

The equilibrium crystal dissolution temperature $T_d°$ for fully grown crystals was determined by differential scanning calorimetry (Perkin-Elmer DSC-7) using a method by Organ and Keller.[29] For these measurements dust-free PEO solutions at 0.1% were prepared, seeded, and grown at fixed crystallization temperatures, T_c. Approximately 50 μL of crystal suspension was sealed in a high-pressure aluminum DSC sample pan. The sample was kept very close to T_c at all times and the DSC run was begun near T_c at a heating rate of 5.0 °C min^{-1}, as used by Organ and Keller to minimize superheating and additional crystal thickening.[29] For each molecular weight of PEO, $T_d°$ was measured from the DSC peak at several crystallization temperatures covering as broad a range as possible.

Results

The fluctuation of scattering intensity from a suspension of randomly diffusion particles provides an intensity–intensity homodyne autocorrelation function of the form

$$G^{(2)}(\tau) = A \exp(-2\Gamma\tau + \Gamma_2\tau^2) + B \quad (4)$$

where A is an instrument optical constant, B is the mean background intensity, and Γ and Γ_2 are the first two terms of a cumulant expansion where the decay constant Γ is related to the diffusion coefficient of the scattering species as

$$\Gamma = Dq^2 \quad (5)$$

The scattering angle (40° in these studies) defines the value of q as

$$q = (4\pi n/\lambda_o) \sin(\theta/2) \quad (6)$$

where n is the refractive index (1.494) and λ_o is the laser wavelength (514.5 nm).

The translational diffusion coefficient D is the primary quantity determined by DLS. D can be related to the hydrodynamic radius R_h through the Stokes–Einstein equation

$$D = kT/6\pi\eta R_h \quad (7)$$

with k the Boltzman constant, T the temperature, and η the solvent viscosity. For a solid spherical particle R_h is equal to the particle radius. The morphology of PEO crystals grown from a toluene solution is a cluster of stacked square lamellae with a height less than its diameter (Figure 1).[21] This means that R_h describes an object resembling an oblate ellipsoid with major axis a and minor axis b. Equation 7 is thus modified to read

$$D = kT\phi/6\pi\eta a^{2/3}b^{1/3} \quad (8)$$

where ϕ is a function[30] depending only on the axial ratio $\rho = a/b$ as

$$\phi = \frac{\rho^{2/3}}{(\rho^2-1)^{1/2}} \arctan(\rho^2-1)^{1/2} \quad \text{for } \rho > 1 \quad (9)$$

The effective hydrodynamic radius is $R_h = a^{2/3}b^{1/3}/\phi$.

The crystal growth rate can be expressed as the first derivative of the linear dimension (the major axis a) of the crystal with respect to time, da/dt. This can be related to the experimentally measurable quantity dR_h/dt as

$$\frac{dR_h}{dt} = \frac{d}{dt}\left(\frac{\rho^{2/3}b}{\phi}\right) = \frac{\rho^2(\rho^2-1)^{-1/2}\arctan(\rho^2-1)^{1/2} - 1}{\rho[\arctan(\rho^2-1)^{1/2}]^2}\frac{da}{dt} = Y\frac{da}{dt} \quad (10)$$

where the function Y depends on ρ. For this equation the assumption has been made that b remains constant during the crystal growth, i.e., that the crystal thickness does not change. This assumption is supported by the observations of Organ and Keller,[29] who found no evidence of lamellae thickening during isothermal crystal growth from solution, except for a marginal effect at high crystallization temperatures near $T_d°$. In our experiments, it is observed that the fully grown crystals maintain morphology similar to seed crystals, indicating that aggregated crystals are not formed during the crystal growth. Therefore the assumption of fixed thickness in the derivation is acceptable. Even for the seed crystals, ρ is greater than 1. If ρ is 1.2, Y is 0.659. During the process of two-dimensional crystal growth in the plane of the major axes, ρ increases and Y reaches an asymptote at 0.637. Given that it shows such a small variation, Y is therefore treated as a constant and the kinetics of da/dt are equivalent to the dR_h/dt measurements. Furthermore, if there were a small amount of crystal thickening during the growth, it would counterbalance the effects of the small variation in ρ.

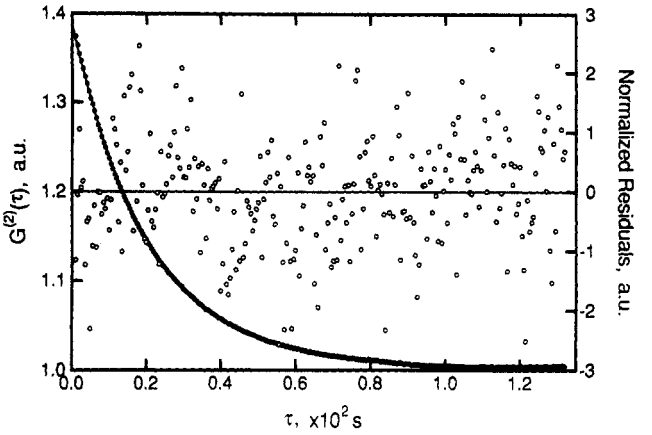

Figure 2. Dynamic light scattering correlation data (●) fit with second-order cumulant function with the normalized residuals (○) superimposed. $\theta = 40°$, $T = 20.47$ °C, $M_p = 1.05 \times 10^6$.

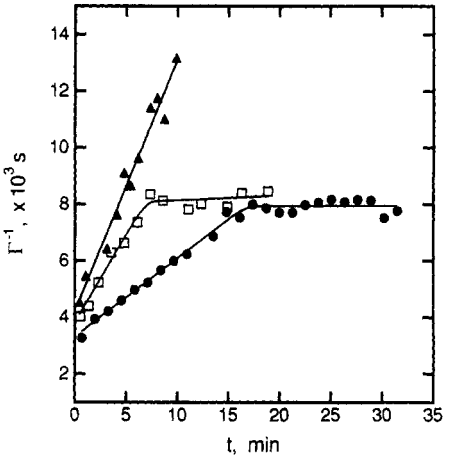

Figure 3. Kinetics of crystal growth monitored by inverse decay constant Γ^{-1} against time for PEO 160 at (●) 20.06 and (□) 18.52 °C and for PEO 770 at (▲) 20.51 °C.

Figure 2 shows typical DLS autocorrelation data (accumulation time 100 s), which is fit to a second-order cumulant expansion with a fixed base line calculated from the correlator monitor channels. The quality of the fit is demonstrated by the corresponding residuals overlay in Figure 2. The ratio $\Gamma_2/\Gamma^2 = 0.2$ is typical of correlation functions obtained for crystal suspensions and indicates a rather monodisperse distribution. Although in the experiments the scattering intensity was not systematically measured for a static light scattering analysis, it was observed that the total intensity increased with crystallization time until crystals were fully grown and then decreased gradually. The decrease of intensity arises from slow sedimentation of the crystals, which have a density greater than that of toluene. This is a potential problem if the particles are polydisperse since larger crystals would sediment first. The cumulant analysis and the fact that DLS measurements of the average crystal size did not change significantly when the fully grown crystals were resuspended by shaking both argue that this effect is negligible. The hydrodynamic uniformity of the crystals is also illustrated by the insensitivity to the data analysis method. Analyses by second or third cumulants or single exponential fitting all produced comparable growth rates.

Applying eqs 5 and 7 to successive DLS accumulations allows the crystal growth to be characterized as in Figure 3, where Γ^{-1} ($\propto R_h$) is shown as a function of time for different molecular weights and crystallization temperatures. Each point in this figure is the result of one DLS autocorrelation function. The crystals grow linearly with

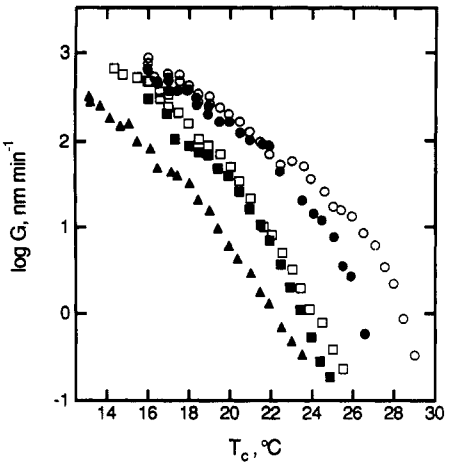

Figure 4. log of crystal growth rate against crystallization temperature for five narrow distribution polymers. (▲) PEO 56, (■) PEO 105, (□) PEO 160, (●) PEO 325, (○) PEO 770.

time initially and reach a plateau when the dissolved polymer is exhausted. The slopes of the linear growth portions of the curves in Figure 3 yield the crystallization rates according to eq 10. In contrast to Point's result,[14] the growth rate is nearly constant until dissolved polymer is exhausted. This is especially true at large supercooling. At shallow supercooling, a slight deviation from linearity in the $1/\Gamma$ vs t plot may be observed. In that case, the initial slope is taken to be the growth rate. The seeds used in this study are ~0.3 μm in diameter, which is small enough to exclude the additional complication discussed by Point et al.[14] that growth rates at high crystallization temperatures are dramatically decreased for large crystal sizes. Point et al.[14] used this reason to explain the decreased growth rate seen in Cooper and Manley's work[31] at low supercooling for large crystals on the order of 2–6-μm diameter.

Figure 4 summarizes the kinetics data as log G plotted against crystallization temperature for various molecular weights. It is clear that, at the same crystallization temperature, longer chains crystallize much faster than shorter chains. This tendency is most obvious at the high temperature end. It should be noted that, for each molecular weight and each concentration, there are experimental limitations on the lower temperature for which the growth rates are accessible by the DLS method. At the lower temperature (larger supercooling) the shortest DLS experiment duration that gave good statistics was ~20 s. Even with this limit there are four decades of growth rate that can be studied for a concentration of 0.01%.

Clearly the kinetics depends strongly on molecular weight and on temperature. To separate these effects, comparisons are made at fixed molecular weight or at constant supercooling, $\Delta T = T_d^\circ - T$. There is a general difficulty in obtaining T_d° precisely for polymer solution crystallization. In our experiment, T_d° is determined for each polymer molecular weight by the method of Organ and Keller using differential scanning calorimetry.[29] The method uses measurements of the dissolution temperature T_d by DSC for PEO crystals that have been grown in toluene at different crystallization temperatures T_c. The data are plotted as T_d vs T_c and extrapolated to an intersection, T_d°, on the $T_d = T_c$ line. It should be pointed out that this method of calculation of T_d° bears uncertainty and tends to yield lower values than other methods.[29] For PEO, the temperature variation of T_d is very small compared with PE. When molecular weight varies from 56 300 to 325 000 and the total range of T_c for the DSC

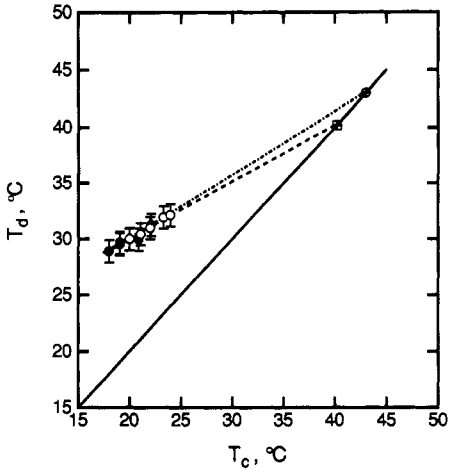

Figure 5. Differential scanning calorimetry measurement of dissolution temperature, T_d, plotted against the temperature of crystallization from solution, T_c, and extrapolated to the $T_d = T_c$ line. The intersection gives an estimate of T_d°. (□) PEO 56, (○) PEO 105.

Table II
Molecular Weight Dependence of Equilibrium Melting and Dissolution Temperatures of PEO Crystals

sample	T_m° calcd, K	T_d° by DSC, K	T_d° adj,[a] K	T_d° adj,[b] K
PEO 56	341.4	313.4 ± 3	312.2	309.5
PEO 105	341.7	316.2 ± 3	313.3	311.4
PEO 160	341.9	315.3 ± 3	313.7	312.2
PEO 325	342.0	313.2 ± 4	314.1	313.3
PEO 770	342.2		314.2	314.2

[a] T_d° is adjusted to resemble T_m° of PEO. [b] T_d° is adjusted to resemble T_d° of PE crystals from p-xylene.

measurements is from 15 (PEO 56) to 27 °C (PEO 325), T_d changes by only 6 °C. For any individual molecular weight sample, T_d will not change more than 3 °C at measurable T_c ranges (see as an example, Figure 5). As molecular weight increases, this T_d range narrows. Such a narrow dissolution temperature range falls into the vicinity of experimental error limit and makes accurate determination of T_d° difficult. The small variation of T_d would introduce significant uncertainties in determining T_d° by the recommended plot of T_d vs $1/l$, where l is the crystal thickness.[29] In previous work, unique behavior of solution-grown PEO crystals was also reported by Shimada et al.[32] They found that when PEO (MW = 0.74, 1.55, 1.87, and 2.33×10^4) crystallizes from 0.05% solution in xylene, the crystal thickness increases with T_c but the melting temperature is not correlated with T_c.

The T_d° values determined from the method shown in Figure 5 are given in Table II, along with an estimate of their rather large uncertainty. For comparison Table II also lists values of $T_m^\circ(N)$, the equilibrium melting temperature as a function of degree of polymerization, which is used by Cheng et al.[9] to describe their PEO crystals. For a degree of polymerization similar to the ones used in this study

$$T_m^\circ(N) = T_m^\circ \frac{N\Delta h_f - \sigma_e(1 + \alpha T_o)}{N\Delta h_f + RT_m^\circ \ln(N) - \alpha\sigma_e T_m^\circ} \quad (11)$$

where the heat of fusion of the crystal, Δh_f, is 8.67 kJ/mol, T_m° = 342.2 K, α is taken to be 1.29×10^{-2} K^{-1}, and the surface free energy of extended chain crystals σ_e, is 6.57 kJ mol^{-1} in the vicinity of the reference temperature, T_o, of 334.4 K. In order to find temperature and molecular weight dependence of crystal growth, the possible T_d° values for PEO are estimated to follow either T_m° for PEO

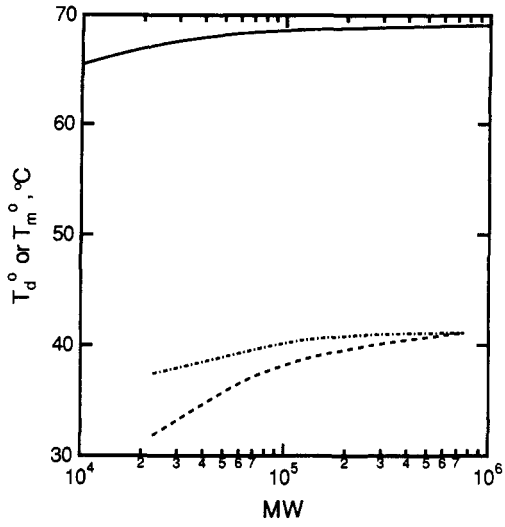

Figure 6. $T_d°$(- · -) of PEO in toluene following $T_m°$ (—) of PEO crystals or $T_d°$ (- - -) following $T_d°$ of PE crystals grown from *p*-xylene.

or according to the semiempirical relation for $T_d°$ in *p*-xylene.[33] The reliability of $T_d°$ is judged by the values of σ_e, which have been reported in the literature.[24,34] For polyethylene crystals, Sanchez and DiMarzio reported[33] $T_m°$ and $T_d°$ from *p*-xylene, which are using the Flory–Vrij estimate[35] and Pennings estimate,[36] respectively. These results show that $T_d°$ increases faster than $T_m°$ with molecular weight. $\Delta T_d°$ is ~5 °C while $\Delta T_m°$ is less than 2 °C when the molecular weight of PE is in the same range as our PEO (from 56 300 to 770 000). Prasad and Mandelkern have developed a relation for dilute solutions,[37] which is similar to conventional ones. Experimental determinations of the equilibrium dissolution temperature for low molecular weight polyethylene fractions (M_n = 575–2900) confirm their major theoretical expectations. However, no work has been reported on whether the relationship still holds when the molecular weight is moderate or high. A similar relationship for PEO has not been reported. The experimental limitation may arise from the difficulty in obtaining extended chain crystals for high molecular weight fractions. The final two columns in Table II give two sets of adjusted $T_d°$ values. The first resembles $T_m°$ of PEO (eq 11) with ~2 °C difference over this range of molecular weight, and the second is modeled after $T_d°$ of PE where there is ~5 °C difference. The two columns are also plotted in Figure 6 along with a plot of eq 11 with Kovacs' estimation of $T_m°$ for infinite molecular weight PEO.[38] Because of the scatter in the individually measured $T_d°$ values, we have used these adjusted $T_d°$ values to define the extent of supercooling ΔT and discuss our results in terms of these two different sets of $T_d°$. It is found that the possible variations of $T_d°$ can have an important influence on quantities such as σ_e and the ratio of the slopes from regime II and I or on the molecular weight dependence of growth kinetics.

As a further comparison to the DSC experiments, we used light scattering to check the dissolution temperature range. Fully dissolved PEO–toluene solutions (0.01% concentration) show very low light scattering compared with pure toluene. When the temperature of a crystal suspension is raised toward the melting point of the crystals, the scattering intensity decreases to the background level. Temperature control of our light scattering instrument is accurate but not conveniently programmable. When the temperature was increased stepwise, it was found, for example, that T_d for PEO 325 crystals grown from 25 °C was less than or equal to 35.3 °C. However,

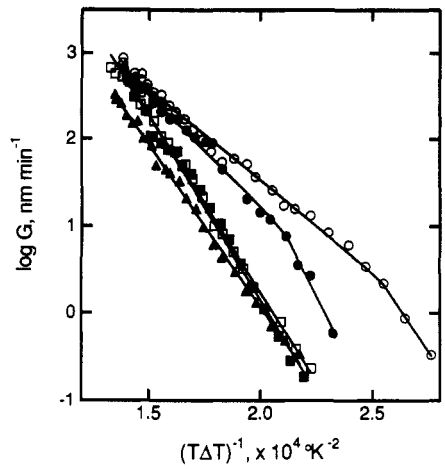

Figure 7. log of crystal growth rate against supercooling $(T\Delta T)^{-1}$ for five narrow distribution polymers. (▲) PEO 56, (■) PEO 105, (□) PEO 160, (●) PEO 325, (○) PEO 770. $T_d°$ estimate based on Kovacs' equation. Lines represent least-squares fits.

the measured value of T_d depended on thermal history and heating rate. When a crystal suspension was held at some temperature below 35.3 °C, for example 33.7 °C, overnight, the scattering intensity was dramatically attenuated but did not totally disappear. When the temperature was raised to 35.3 °C, the intensity decreased further but still remained higher than background. The intensity was then steady for ~5 h and did not completely disappear until the temperature was raised to 36 °C. Such behavior is typical of partial melting and thickening, which occur near T_d. The application of light scattering to measure $T_d°$ does not appear to be any better than DSC.

Discussion

Given the uncertainty in $T_d°$, our discussion of the crystal growth data will be divided into two sections. First the molecular weight dependence of $T_d°$ will be taken from Table II to follow that observed for $T_m°$ of PEO. This implies a small change in $T_d°$ (~2 °C). The second analysis will be based on $T_d°$ values which correlate with measurements of polyethylene crystals grown from *p*-xylene solution. Here a ~5 °C variation is observed over the molecular weight range.

Our original expectation was that there would be only a small variation in $T_d°$ with molecular weight for these long chains. However, we shall see that by accepting the broader variation in $T_d°$ the analysis for molecular weight dependence of crystal growth rates is more consistent with current theoretical predictions.

$T_d°$ following $T_m°$ for PEO. Figure 7 shows the usual Lauritzen–Hoffman plot of logarithm of growth rate vs $(T\Delta T)^{-1}$ of PEO. The data demonstrate that growth rate increases with extent of supercooling and with increasing molecular weight. Furthermore, the dependence of log G on $(T\Delta T)^{-1}$ has a different form for high and intermediate molecular weight as shown by the least-squares fits in Figure 7. For the two highest molecular weights (PEO 325 and PEO 770) two linear regions are observed, while for the lower pair (PEO 56 and PEO 105) a single least-squares line is sufficient. For PEO 160, a regime transition might be seen at deep supercooling. Since the rate measurements here are at the upper limit of our present technique, this transition remains uncertain and further discussion on the transitions will focus mainly on the two highest molecular weights. Our application of "kinked" fits is suggested by previous observations of melt and solution kinetics[2,19] and from the regime transition predictions of nucleation theory.[2]

Table III
Kinetic Parameters Obtained When $T_d°$ Follows $T_m°$ for PEO

sample	regime	ΔT_{I-II}, K	ratio of slopes I/II	$10^{-4}K_g$, K^2	σ_e, erg cm^{-2}
PEO 56	I			8.59	47.16
PEO 56	II			8.59	94.32
PEO 105	I			9.81	53.66
PEO 105	II			9.81	107.33
PEO 160	I			9.39	51.30
	II			9.39	102.59
PEO 325	I			11.79	64.33
	II	16.1	1.96	6.01	65.59
PEO 770	I			8.94	48.77
	II	13.3	1.84	4.86	53.03

As discussed earlier, the theory predicts that the change in K_g will result in a factor of 2 change in the slopes of these lines as the system passes from regime II to either regime I or regime III. For the PEO 325 and PEO 770 data, the ratios of the two slopes are close to 2 (2.0 and 1.8, respectively), and because the transition is from lower slope to higher slope as the supercooling decreases (toward the right), this may be identified as a regime II to regime I transition. The transition occurs at $\Delta T = 16.1 \pm 0.5$ K for PEO 325 and $\Delta T = 13.3 \pm 0.5$ K for PEO 770. For PEO crystallized from melt, Cheng et al.[9] found $\Delta T_{I-II} = 10.0 \pm 0.5$ K for intermediate molecular weights. Allen and Mandelkern[8] found an average ΔT_{I-II} of ~24 K for molecular weights up to 9.5×10^5. Since they chose a much higher $T_m°$ of PEO than did others,[9,24] ΔT_{I-II} should be adjusted accordingly. Hence it falls around $\Delta T = 13$ K. Our values of ΔT_{I-II} are slightly higher than these two melt results. For the polyethylene case ΔT_{I-II} is ~17.5 K for melt crystallization, while it is 19.8 and 22.4 K for PE crystallization from tetradecanol and hexadecane, respectively.[19]

At first sight the identification of regimes for the three intermediate molecular weights seems difficult because they lie parallel to neither the regime I lines nor the regime II lines assigned above. However, further analysis shows that they resemble regime I growth. This assessment is demonstrated quantitatively by the data in Table III where K_g's, the slopes of log G vs $(T\Delta T)^{-1}$ according to eq 3, are listed and σ_e's, the folding surface free energies, are calculated from K_g based on regime I and II expressions (eq 2), using $b = 0.465$ nm,[2] $\Delta h_f = 2.31 \times 10^9$ erg cm^{-3},[34] $\sigma = 10$ erg cm^{-2},[34] and $T_d°$ replacing $T_m°$ for growth from solution. The calculated σ_e values given in Table III are in the vicinity of 56.5 ± 9 erg cm^{-2}, if we assign the intermediate molecular weight samples to regime I. It is obvious that regime II is not reasonable, since σ_e would be even higher than that for PE and would not agree with data from other sources.[24,34] Kovacs has reported σ_e increasing with molecular weight in melt crystallization studies of PEO.[24] Our values are comparable to those for this range of molecular weights ($45 < \sigma_e < 60$ erg cm^{-2} assuming $\sigma \approx 10$), obtained from growth rate data or from melting point measurements.[24,34]

The work of chain folding, q, can be obtained from the surface free energy by $q = 2ab\sigma_e$, where the stem width a is taken as 0.467 nm.[2] The result, $q = 3.5 \pm 0.5$ kcal mol^{-1}, is close to but smaller than q for polyethylene,[2] which is 5.06 kcal mol^{-1}, and presumably this reflects the more flexible nature of PEO chains.

We further applied Lauritzen "Z test",[39] which involves the dimensionless parameter

$$Z = iL^2/4g \tag{12}$$

to evaluate our data. Z should be less than 0.1 at crystallization temperatures in regime I, $^1/_2$ at T_{I-II}, and unity or greater in regime II. From $G_I = biL$ and eq 3 one could get

$$i_{I-II}\ (\text{nuclei nm}^{-1}\ \text{s}^{-1}) = \frac{G_{I-II}}{bL} = i_o(\Delta T)\exp\left(\frac{-U^*}{RT_{I-II}}\right)\exp\left(\frac{-K_g}{T_{I-II}\Delta T_{I-II}}\right) \tag{13}$$

where the preexponential factor has included a weak temperature-dependent term ΔT_{I-II}. To evaluate i_{I-II} and i_o we use $U^* = 2000$ cal/mol, typical of the diffusion energy of a polymer in dilute solution, and we let $L = 500$ Å by assuming that L for PEO and polyethylene crystals fall in the same range.[11] K_g and T_{I-II} come from our experiment. For PEO 325, i_{I-II} and i_o are calculated as 2.9×10^{-3} nuclei nm^{-1} s^{-1} and 2.4×10^8 nuclei nm^{-1} s^{-1} K^{-1}, respectively. For PEO 770, i_{I-II} and i_o are 1.14×10^{-3} nuclei nm^{-1} s^{-1} and 1.23×10^7 nuclei nm^{-1} s^{-1} K^{-1}. At other temperatures, i can be calculated by replacing T_{I-II} in eq 13 with T. Likewise, g_{I-II} can be calculated immediately from $G_{II} = b(2ig)^{1/2}$ as

$$g_{I-II} = G_{I-II}^2/2b^2i \quad \text{at } T_{I-II}$$

Since[3]

$$g_{I-II} = g_o(\Delta T_{I-II})\exp\left(\frac{-U^*}{RT_{I-II}}\right)\exp\left(\frac{-q}{RT_{I-II}}\right) \tag{14}$$

and q is known from our experiment, we find $g_{I-II} = 3.5$ nm s^{-1} and $g_o = 2.3 \times 10^3$ nm s^{-1} K^{-1} for PEO 325. For PEO 770, $g_{I-II} = 1.41$ nm s^{-1} and $g_o = 5.06 \times 10^2$ nm s^{-1} K^{-1}. By putting all the constants in

$$g = g_o(\Delta T)\exp\left(\frac{-U^*}{RT}\right)\exp\left(\frac{-q}{RT}\right) \tag{14'}$$

the Z test could be performed and the results are plotted in Figure 8. At T_{I-II}, $Z = 0.5$. From lower to higher temperatures, Z decreases dramatically from values much greater than 1 to less than 0.1. By use of i and g, the mean separation of nucleation along the growth face can be calculated:

$$S_k = (2g/i)^{1/2} \tag{15}$$

At T_{I-II}, S_k is found to be very close to L (~500 Å).

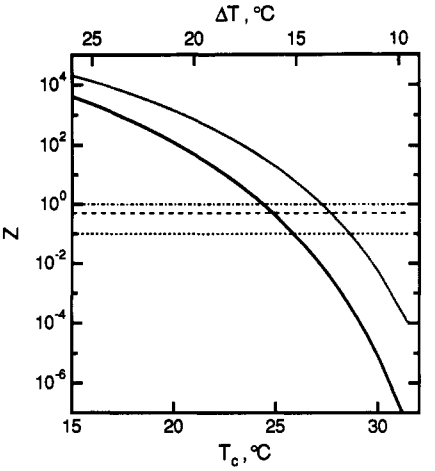

Figure 8. Lauritzen Z test for PEO 325 (—) and PEO 770 (···). Three horizontal lines correspond to $Z = 1$, $Z = 0.1$, $Z = 0.5$.

$T_d°$ following $T_d°$ for PE. As discussed above we have the option of modeling $T_d°$ after $T_d°$ of polyethylene crystallized from xylene rather than after $T_m°$ for PEO. The questions will be whether the kinked regime transition curves are still observed and whether the molecular weight

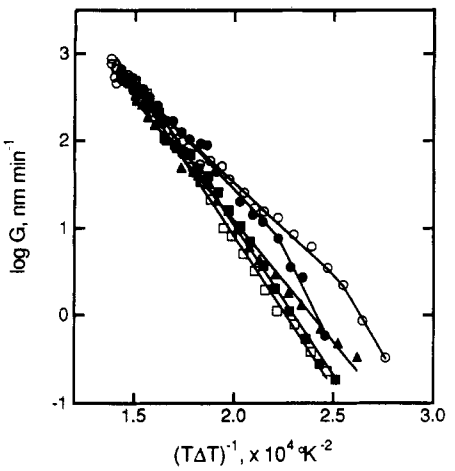

Figure 9. log of crystal growth rate against supercooling $(T\Delta T)^{-1}$ for five narrow distribution polymers. (▲) PEO 56, (■) PEO 105, (□) PEO 160, (●) PEO 325, (○) PEO 770. $T_d°$ estimate based on Sanchez–DiMarzio work for PE. Lines represent least-squares fits.

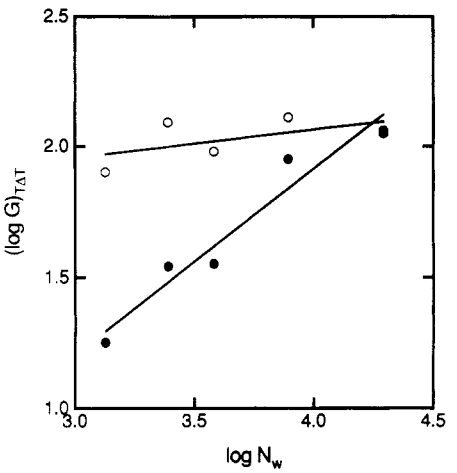

Figure 10. Power law dependence of growth rate on degree of polymerization is demonstrated by slopes of log G against log N_w at constant supercooling ($1/T\Delta T = 1.6 \times 10^{-4}$ K^{-2}) when $T_d°$ is estimated from Kovacs' equation (●) or from the Sanchez–DiMarzio work for PE (○).

Table IV
Kinetic Parameters Obtained When $T_d°$ Follows $T_d°$ for PE Crystals Grown in *p*-Xylene

sample	regime	ΔT_{I-II}, K	ratio of slopes I/II	$10^{-4}K_g$, K^2	σ_e, erg cm^{-2}
PEO 56	II			5.24	58.0
PEO 105	II(I)			7.84	86.2
PEO 160	II (I)			7.96	87.4
PEO 325	I			10.55	57.7
	II	15.3	1.91	5.52	60.4
PEO 770	I			8.94	48.8
	II	13.3	1.84	4.86	53.0

dependence of growth rate changes sign. The data in Table II indicate that this treatment implies more variation of $T_d°$ over our molecular weight range. Such variation is supported by DiMarzio's estimation of $T_d°$ as a function of molecular weight even in this high molecular weight range.[33]

Figure 9 is a plot of log G vs $1/T\Delta T$ where $\Delta T_d°$ varies ~4.6 °C for these mass fractions. The dependence of log G on $(T\Delta T)^{-1}$ again shows a different form for high and intermediate molecular weight. For the two highest molecular weights (PEO 325 and PEO 770) two linear regions may be observed, while for the lower fractions (PEO 56, PEO 105, and PEO 160) a single least-squares line is sufficient. The slope differences of two sets of kinked curves (PEO 325 and PEO 770) are 1.9 and 1.8, respectively, when the same breaking points are chosen as in Figure 7. From the direction of the breaks, we again identified regime I growth at low supercooling for this pair and regime II kinetics at high supercooling. This is in agreement with the previous analysis. By use of the same σ, b, and Δh_f but new $T_d°$ values, σ_e values are calculated and they are given in Table IV. For the two high molecular weights, σ_e's from both regimes are in the range 55 ± 5 erg cm^{-2}. Likewise if PEO 56 is interpreted as regime II growth its σ_e is consistent. However, for PEO 105 and PEO 160 the σ_e values are small if they are calculated for regime I growth and too large if calculated as regime II growth. These results actually exhibit the tendency for low molecular weight to show regime II kinetics, while as chain length increases the growth contains a mixture of both regimes. Finally, regime segregation is seen for high molecular weight samples. This tendency was not obvious when the data were interpreted using $T_d°$ following $T_m°$ for PEO.

Molecular Weight Dependence of the Growth Rate. The molecular weight dependence of the actual growth rate can also be discussed. Here we find results that are unexpected under the kinetic theory model and in comparison to experimental results for bulk crystal growth. Figure 10 demonstrates the scaling of the growth rate with degree of polymerization. In this figure, log G vs log N_w is plotted at fixed supercooling of $(T\Delta T)^{-1} = 1.6 \times 10^{-4}$ with both estimations of $T_d°$. When $T_d°$ is taken to follow $T_m°$ for bulk PEO (filled circles) the data follow a line with the slope corresponding to $-\alpha$ from eq 3 that is equal to 0.8. For the same data plotted with $T_d°$ taken to follow the behavior for PE in xylene (open circles), the molecular weight dependence is much weaker with a slope corresponding to 0.1.

Because the lines in Figures 7 and 9 are not exactly parallel, the molecular weight dependence from these data will vary with the chosen supercooling. Nevertheless, when data are taken from Figure 7, the slope is always positive and the magnitude increases for lower supercooling. For data from Figure 9, the slope will be either slightly positive or slightly negative depending on the degree of supercooling. Strictly speaking, the plot of log G vs log N_w at fixed $T\Delta T$ is not quite correct because $K_g/T\Delta T$ has a slight dependence on molecular weight. We have chosen to neglect this effect because, as is apparent in Tables III and IV, the uncertainty in K_g even when the regime is unambiguous leads to a great deal of scatter. We note that previous workers have also neglected the molecular weight dependence of K_g.[3,9]

DiMarzio et al.[6] have estimated the dependence of the nucleation process on chain length as near $N^{-1/2}$ for crystallization from solution. This in turn predicts a very small negative molecular weight dependence for crystal growth rate in both regimes. The model describes a chain pulled by a force at one end through a small hole in a surface. This is in contrast to melt theory where the constraint of reptation is applied to chain motion. The reptation constraint leads to a strong $N^{-1.42\pm0.08}$ prediction for regime I and $N^{-1.21\pm0.04}$ for regime II. Although the experimental data have some scatter, results for polyethylene have quantitatively confirmed these predictions.[3] Data for bulk crystallization of poly(ether–ether–ketone) also agree with the predictions qualitatively.[40] In dilute solution, where the motion of the chain is not constrained to be along its tangent, the molecular weight dependence should be less. Even so, it is difficult to reconcile the analogy with the observation of positive molecular weight

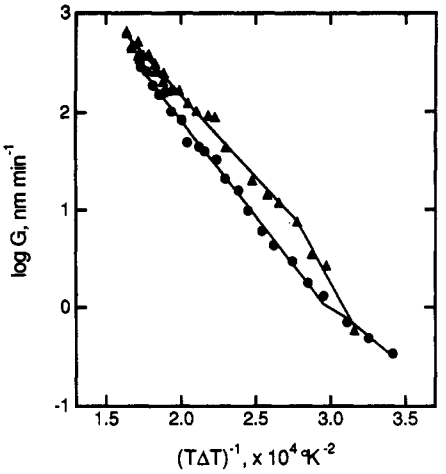

Figure 11. Plot of log G vs $1/T\Delta T$ for PEO 56 (●) and PEO 325 (▲) as $T_d°$ decreases 3 °C. Notice a reverse II–I transition for PEO 56.

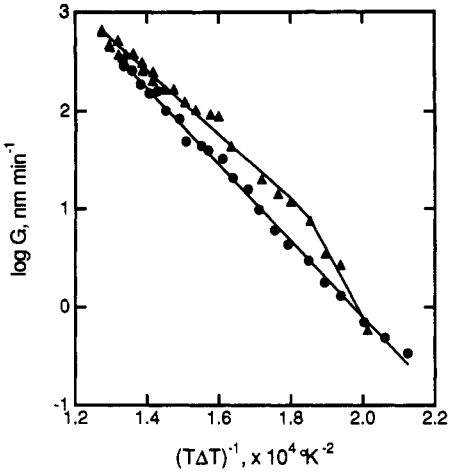

Figure 12. Plot of log G vs $1/T\Delta T$ for PEO 56 (●) and PEO 325 (▲) as $T_d°$ increases 3 °C.

dependences. We note that the z-average chain length has typically been used in the previous work. Even though for polydisperse systems (unlike those used for these studies) this can cause a change in the magnitude of α, the sign will not be affected. Clearly the observed positive molecular weight dependence requires theoretical explanation or it points to a major failure resulting from our choice of $T_d°$.

Comparisons to solution experiments are difficult because there is not much data available. We observe in the polyethylene work of Organ and Keller[18] a slight increase of crystal growth rate with molecular weight at lower supercooling. Leung et al.[41] found that for low molecular weight polyethylene (M_w from 3100 to 22 600) crystallized from xylene a plot of log G vs log M decreased at the beginning and then increased dramatically. The authors did not pursue an explicit functional dependence. On the other hand, Cooper and Manley's data[31] showed that at constant supercooling intermediate molecular weight PE crystallized from a dilute solution of xylene showed a negative dependence. This would seem to be some of the only data in accord with the theoretical expectations.

It is obvious that the choice of $T_d°$ makes some difference in the interpretation of crystallization kinetics. It affects the molecular weight dependence of growth rate, the σ_e values, and, for intermediate molecular weights, the assignment of regimes. Nevertheless, for high molecular weights, regime transitions are clearly identified. Given the uncertainty in assigning $T_d°$, one may wonder if the regime transition would disappear if $T_d°$ were varied up or down by several degrees. Figures 11 and 12 are plots of log G against $1/T\Delta T$ for PEO 56 and PEO 325 as typical data sets where $T_d°$ has been decreased 3 °C and increased 3 °C, respectively. As $T_d°$ decreases, the plots tend to bend upward. This is illustrated in Figure 11 by the apparent reverse regime II–I transition for PEO 56 and the small ratio (1.7) of regime II–I transition for PEO 325. Table V shows that the slopes in these plots decrease significantly and hence σ_e decreases with lower $T_d°$. This coincides with Cheng's finding of a reverse regime II–I transition at very low supercooling and systematically low σ_e values for intermediate molecular weight PEO crystals grown from melt.[9] It should be noted that a supposed $T_d°$ as low as 33.4 °C for PEO 56 seems unacceptable in light of our measured dissolution endotherms for PEO 56. As an extreme example, our highest one peaks at 32.4 °C and does not fully disappear until ~34 °C. For chain-folded crystals, $T_d°$ cannot be measured, but is extrapolated; and is always higher than the measured T_d by several degrees. It is possible that the so-called reverse transition may result from the choice of $T_m°$ that is too low.

Table V
Kinetic Parameters Obtained When $T_d°$ Is Chosen at Extremes of Reasonable Limits

sample	$T_d°$, K	regime	ΔT_{I-II}, K	ratio of slopes I/II	$10^{-4}K_g$, K^2	σ_e, erg cm^{-2}
PEO 56	306.5	I(II)	11.5	1.58	4.55	25.4
		II(I)			2.89	32.3
PEO 325	310.3	I	12.3	1.69	6.51	36.0
		II			3.86	42.6
PEO 56	312.5	I			8.92	48.9
PEO 325	316.3	I	18.3	2.09	15.61	84.6
		II			7.48	81.1

Experiments are presently underway in our laboratory to investigate the concentration dependence for the PEO–toluene system and to apply this technique to crystallization with different polymer–solvent pairs. Future studies will extend this work to lower molecular weights where integer folding and extended chain crystals may be formed. Previous work in this area[24-27,42] suggests that the behavior of regime transitions, surface free energies, work of chain folding, and molecular weight dependence of growth may be qualitatively and quantitatively different.

Conclusion

It has been demonstrated in this investigation that kinetic studies of polymer crystallization from solution can be made nonintrusive, instantaneous, and continuous by using dynamic light scattering and a controlled seeding method. Data are obtained to plot crystal size against time and to find the growth rate at a designated crystallization temperature. The method overcomes the temperature delay inherent in self-seeding methods, which can be a serious problem at large supercooling. Several aspects of the kinetics of solution crystallization of five different molecular weights of PEO from toluene have been demonstrated by these experiments.

The initial growth of PEO crystals is linear with time and the growth rate is easily extracted. Plots of log G vs $1/T\Delta T$ for intermediate molecular weights are linear and show no break. For high molecular weights a break could be assigned and two linear regions can be observed with slopes different by roughly a factor of 2. This phenomenon is independent of the choices of $T_d°$, the equilibrium dissolution temperature. For comparison to kinetic nucleation theory, the direction of the break is used to assign the region of shallow supercooling as regime I and the

deep supercooling as regime II for PEO 325 and PEO 770. As in our previous experimental work, a more detailed kinetic analysis of the temperature dependence and any interpretation of the molecular weight dependence both rely strongly on the proper assignment of $T_d°$ for consistent results.

Acknowledgment. We are grateful for helpful discussions with Professors A. Keller and R. Salovey during the beginning stages of these investigations and we thank Professors J. Hoffman and L. Mandelkern for several useful suggestions. We are also grateful for helpful suggestions by a reviewer. This work was supported by the University of Southern California Faculty Research and Innovation Fund.

References and Notes

(1) For a summary, see, for example: Sperling, L. H. *Introduction to Physical Polymer Science*; John Wiley & Sons: New York, 1986; p 177, and references cited.
(2) Hoffman, J. D.; Davis, G. T.; Lauritzen, Jr., J. I. In *Treatise on Solid State Chemistry*; Hannay, N. B., Ed.; Plenum: New York, 1976; p 497.
(3) Hoffman, J. D.; Miller, R. L. *Macromolecules* **1988**, *21*, 3038.
(4) Hoffman, J. D. *Polymer* **1983**, *24*, 3.
(5) Hoffman, J. D. *Polymer* **1982**, *23*, 656.
(6) DiMarzio, E. A.; Guttman, C. M.; Hoffman, J. D. *Faraday Discuss. Chem. Soc.* **1979**, *68*, 211.
(7) Phillips, P. J. *Polym. Prepr. (Am. Chem. Soc., Div. Polym. Chem.)* **1989**, *30*(2), 284.
(8) Allen, R. C.; Mandelkern, L. *Polym. Bull.* **1987**, *17*, 473.
(9) Cheng, S. Z. D.; Chen, J.; Janimak, J. J. *Polymer* **1990**, *31*, 1018.
(10) Lovinger, A. J.; Davis, D. D.; Padden, F. J., Jr. *Polymer* **1985**, *26*, 1595.
(11) Hoffman, J. D.; Miller, R. L. *Macromolecules* **1989**, *22*, 3502.
(12) Roitman, D. B.; Marand, H.; Miller, R. L.; Hoffman, J. D. *J. Phys. Chem.* **1989**, *93*, 6919.
(13) Keller, A.; Pedemonte, E. *J. Cryst. Growth* **1973**, *18*, 111.
(14) Point, J. J.; Colet, M. C.; Dosiere, M. *Polymer* **1986**, *24*, 357.
(15) Toda, A.; Kiho, H. *J. Polym. Sci., Part B: Polym. Phys.* **1989**, *27*, 53.
(16) Picot, C.; Weill, G.; Benoit, H. *J. Colloid Interface Sci.* **1968**, *27*, 360.
(17) Picot, C.; Weill, G. *J. Polym. Sci., Polym. Phys. Ed.* **1974**, *12*, 1733.
(18) Organ, S. J.; Keller, A. *J. Polym. Sci., Part C: Polym. Lett.* **1987**, *25*, 67.
(19) Organ, S. J.; Keller, A. *J. Polym. Sci., Part B: Polym. Phys.* **1986**, *24*, 2319.
(20) Ding, N.; Amis, E. J.; Yang, M.; Salovey, R. *Polymer* **1988**, *29*, 2121.
(21) Ding, N.; Amis, E. J.; Salovey, R.; Briber, R. M. *J. Polym. Sci., Part C: Polym. Lett.* **1989**, *27*, 489.
(22) Organ, S. J.; Keller, A. *J. Mater. Sci.* **1985**, *20*, 1571.
(23) Kovacs, A. J.; Lotz, B.; Keller, A. *J. Macromol. Sci.-Phys.* **1969**, *B3*, 385.
(24) Kovacs, A. J.; Straupe, C.; Gonthier, A. *J. Polym. Sci., Polym. Symp.* **1977**, *59*, 31.
(25) Kovacs, A. J.; Straupe, C. *J. Cryst. Growth* **1980**, *48*, 210.
(26) Cheng, S. Z. D.; Bu, H. S; Wunderlich, B. *Polymer* **1988**, *29*, 579.
(27) Sadler, D. M. *J. Polym. Sci., Polym. Phys. Ed.* **1985**, *23*, 1533.
(28) Seery, T. A. P.; Shorter, J. A.; Amis, E. J. *Polymer* **1989**, *30*, 1197.
(29) Organ, S. J.; Keller, A. *J. Mater. Sci.* **1985**, *20*, 1602.
(30) Scheraga, H. A. *Protein Structure*; Academic Press: New York, 1961.
(31) Cooper, M.; Manley, R. St. J. *Macromolecules* **1975**, *8*, 219.
(32) Shimada, T.; Okui, N.; Kawai, T. *Makromol. Chem.* **1980**, *181*, 2643.
(33) Sanchez, I. C.; DiMarzio, E. A. *Macromolecules* **1971**, *4*, 677.
(34) Pracella, M. *Eur. Polym. J.* **1985**, *21*, 551.
(35) Flory, P. J.; Vrij, A. *J. Am. Chem. Soc.* **1963**, *85*, 3548.
(36) Pennings, A. J. *J. Polym. Sci., Part C: Polym. Symp.* **1967**, *16*, 1799.
(37) Prasad, A.; Mandelkern, L. *Macromolecules* **1989**, *22*, 914.
(38) Buckley, C. P.; Kovacs, A. J. In *Structure of Crystalline Polymers*; Hall, I. H., Ed.; Elsevier: New York, 1984; p 261.
(39) Lauritzen, J. I. *J. Appl. Phys.* **1973**, *44*, 4353.
(40) Deslandes, Y.; Day, M.; Roovers, J. *Polym. Prepr. (Am. Chem. Soc., Div. Polym. Chem.)* **1989**, *30*(2), 305.
(41) Leung, W. M.; Manley, R. S. J.; Panaras, A. R. *Macromolecules* **1985**, *18*, 760.
(42) Hoffman, J. D. *Macromolecules* **1986**, *19*, 1124.